

## On the instantaneous frequency and quality factor

José M. Carcione,<sup>1</sup> Davide Gei,<sup>1</sup> Stefano Picotti<sup>1</sup> and Marco A.B. Botelho<sup>2,\*</sup>

<sup>1</sup>*National Institute of Oceanography and Applied Geophysics (OGS), 34010 Sgonico, TS, Italy. E-mail: [dgei@ogs.trieste.it](mailto:dgei@ogs.trieste.it)*

<sup>2</sup>*Instituto de Geociencias/CPGG, Universidade Federal da Bahia, Campus Universitario de Ondina, Salvador 40170-110, BA, Brazil*

Accepted 2021 June 30. Received 2021 June 23; in original form 2021 May 12

### SUMMARY

We analyse the concepts of instantaneous frequency (IF) and quality factor (IQ). It is verified that the time-averaged IF is equal to the centroid of the signal energy of the spectrum and that the centroid of the signal spectrum is equal to the IF at the peak of the signal envelope. The latter property can be used to obtain the frequency shift required by tomographic methods. Then, we analyse the two-tone stationary Mandel signal in the lossless and lossy cases. The IQ is not infinite in the lossless case, although its reciprocal average vanishes, and the lossless and lossy IFs at the peak of the signal envelope are the same, whereas the IQ at this peak depends on the amplitudes and quality factors of the tones. The IQ of a propagating Ricker wavelet has a singularity at the peak of the envelope, which shows a shift in the lossy case, related to the velocity dispersion. We consider a lossy layer described by the Zener model. Varying its thickness implies a large variation in the IF, introducing unphysical spikes when the top and bottom reflections of the layer start to overlap. Finally, a practical application to real seismic data is presented.

**Key words:** Time-series analysis; Computational seismology; Seismic attenuation.

### 1 INTRODUCTION

Seismic traces exhibit time-varying frequencies, which are usually interpreted with spectrograms (Qadrouh *et al.* 2016), wavelet transforms (Sinha *et al.* 2005) and the concept of instantaneous frequency (IF) (Barnes 1991, 1993; Boashash 1992; Matheny & Nowack 1995; Xing *et al.* 2019). The IF is the time derivative of the phase of the complex trace, which is a complex continuation of the real trace, where the imaginary part is the Hilbert transform of the real signal (Taner *et al.* 1979; Cohen 1995). The complex trace in exponential form basically separates amplitude (envelope) from phase. The IF has been used to define ‘low-frequency shadows’ (LFSs), generally interpreted as seismic attenuation due to the presence of gas (e.g. Geletti & Busetti 2011). However, according to Barnes (2013), only few cases of LFSs are convincing to reveal the presence of gas. Caution is required since the presence of low frequencies may be due to other causes, such as normal moveout (NMO) stretch, which is important at far offset traces (Carcione *et al.* 2018), and not to seismic attenuation (Ba *et al.* 2016, 2019; Pang *et al.* 2019). These phenomena (LFS) also appear in seismic exploration of hydrocarbons related to bright spots, but Castagna *et al.* (2003) state that ‘For every example shown, the shadow was stronger than the reservoir reflection at lower frequencies, suggesting that shadows are not necessarily a simple attenuation

phenomenon because low-frequency energy must have been added or amplified by some physical or numerical process. Attenuation alone should simply attenuate higher frequencies, not boost lower frequencies’. Actually, the LFS may have multiple causes that are not mutually exclusive. Ebro (2004) lists six stack-related causes, such as NMO stretch, two due to intrinsic attenuation, one due to wave interference and another due to improper seismic deconvolution. One of the causes of this misinterpretation is the methodology. Marfurt & Kirilin (2001) show that the simple peak-frequency concept performs better than the IF (see their figs 6 and 7). The problem also appears in the analysis of thin beds. Robertson & Nogami (1984) show that the IF reaches an anomalously high value when the bed thickness is about a quarter period. Although IF may exceed physical values, it is true that this property can be used to identify thin layers. Another concept arising from complex-trace analysis is the instantaneous quality factor (IQ) (Tonn 1991). IQ is claimed to be ‘a physical attribute with a strong relation to porosity, permeability, and fracture’ ([https://wiki.seg.org/wiki/Dictionary:Instantaneous\\_q\\_factor](https://wiki.seg.org/wiki/Dictionary:Instantaneous_q_factor)). However, it is the IF and not the IQ that has been used to estimate  $Q$ . Barnes (1991), Yang & Gao (2009) and Gao *et al.* (2011) estimate  $Q$  from the IF, basically from its value at the envelope peak. A similar method, based on this peak, has been implemented by Engelhard (1996). Gao *et al.* (2011) obtain a similar frequency-shift– $Q$  equation to that of Quan & Harris (1997), based on the spectrum centroid, as expected. Use of the IF avoids the problem of a subjective time windowing of seismic traces. Gao *et al.* (2011) tested the transmission problem (a VSP

\*Deceased from Covid-19.

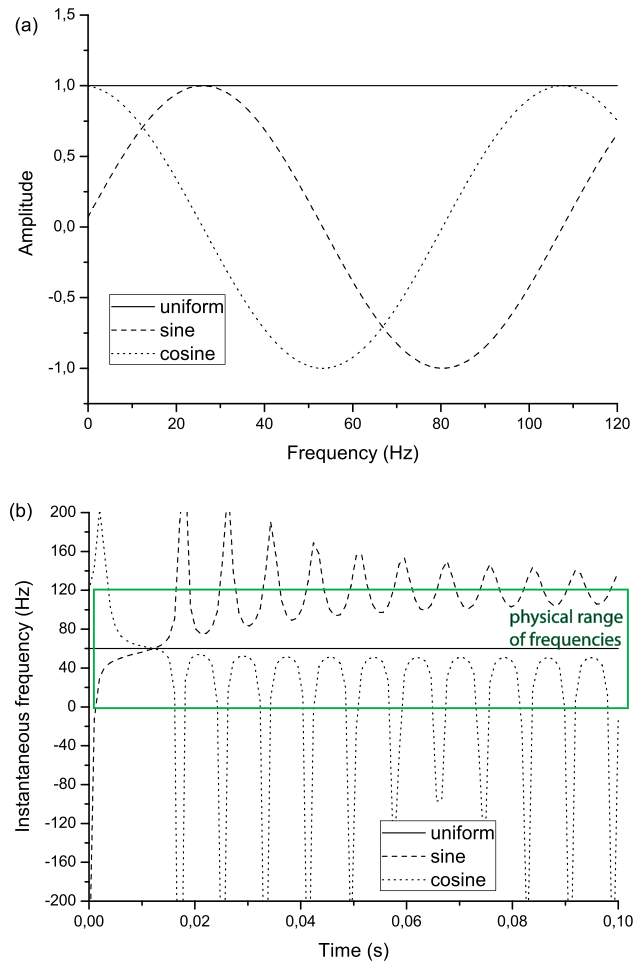


**Figure 1.** (a) Amplitude distribution  $a_j$  and (b) IF of the signal given in eq. (7).

experiment) and found that the frequency-shift method of Quan & Harris (1997) fails near interfaces due to overlapping of the direct wave with reflected waves, whereas the method based on the IF is less sensitive to interference reflections and has a higher resolution. In the presence of noise, Gao *et al.* (2011) use the wavelet transform, instead of the Hilbert transform, to compute the IF, improving in this manner the estimation based on damping parameter (Matheny & Nowack 1995). Wang *et al.* (2013) generalize the IF by introducing fractional time derivatives, showing that an order of 0.99 instead of the first-order derivative yields better results.

Here, we analyse the IF and IQ for the Mandel problem generalized to the anelastic case, a propagating Ricker wavelet in a lossy medium and for the seismic-reflection trace in the presence of a layer. An example with real seismic data is finally presented.

## 2 THE INSTANTANEOUS FREQUENCY

The complex trace of a real signal  $s(t)$  is

$$z(t) = s(t) + i\mathcal{H}[s(t)] = a(t) \exp[i\phi(t)] \equiv \Sigma_2 + i\Sigma_1 \quad (1)$$

(Cohen 1995), where  $i = \sqrt{-1}$ ,  $\mathcal{H}$  is the Hilbert transform operator,  $a(t) = |z|$  is the instantaneous amplitude,  $\phi(t)$  is the instantaneous phase, and  $\Sigma_2$  and  $\Sigma_1$ , respectively, are the real and imaginary parts

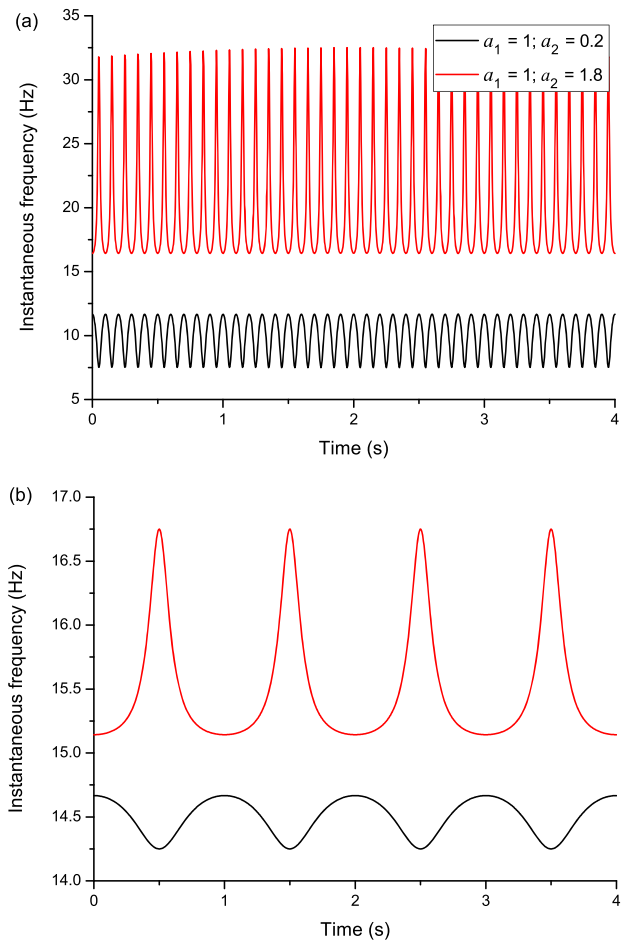


**Figure 2.** IF for the Mandel (1974) example, where  $f_0 = 15$  Hz, (a)  $\Delta f = 5$  Hz and (b)  $\Delta f = 0.5$  Hz. The physical range of frequencies is [10, 20] Hz in (a) and [14.5, 15.5] Hz in (b).

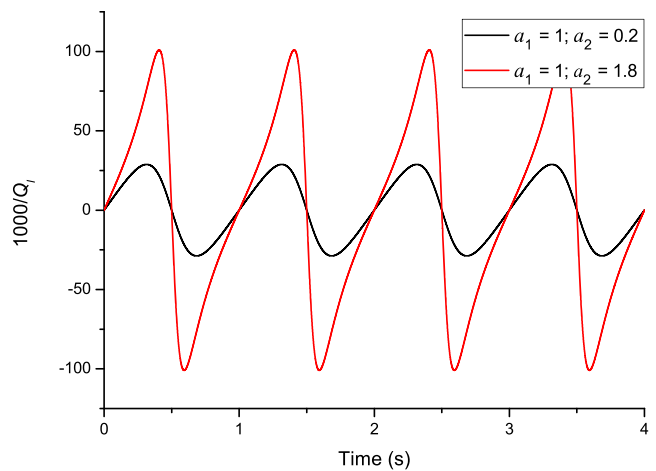


**Figure 3.** Instantaneous attenuation for the Mandel (1974) example, where  $f_0 = 15$  Hz and  $\Delta f = 0.5$  Hz.

of  $z$ . The IF is

$$f_1(t) = \frac{\dot{\phi}}{2\pi} = -\frac{1}{2\pi} i\dot{w}w^* = \frac{\dot{\Sigma}_1 \Sigma_2 - \Sigma_1 \dot{\Sigma}_2}{2\pi(\Sigma_1^2 + \Sigma_2^2)}, \quad w = \frac{z}{|z|}, \quad (2)$$

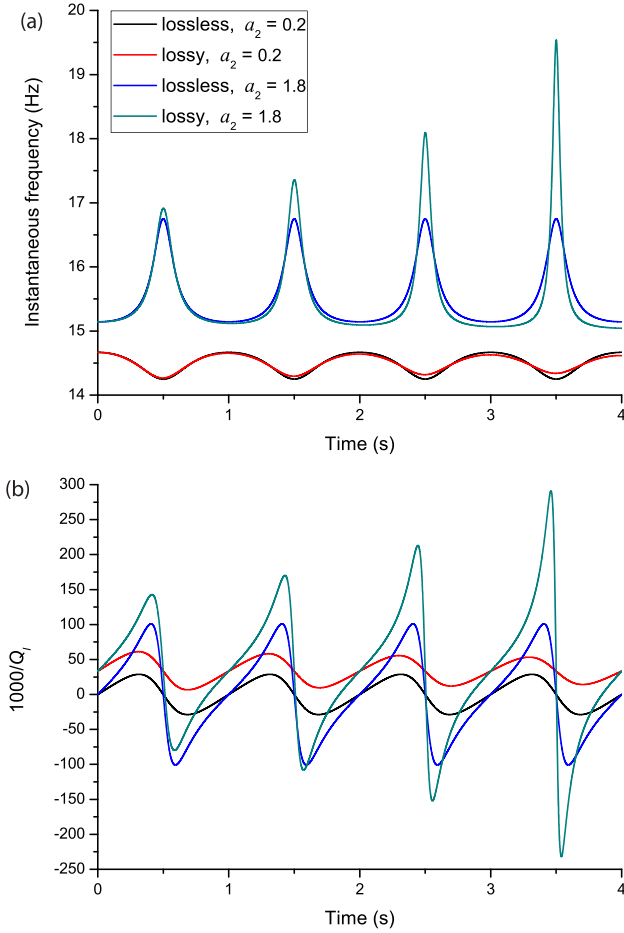


**Figure 4.** (a) IF and (b) IQ for the Mandel example in the lossless and lossy cases, where  $a_1 = 1$ ,  $Q_1 = Q_2 = 30$ ,  $f_0 = 15$  Hz, and  $\Delta f = 0.5$  Hz.

which is eq. (12) in Barnes (2007), where the asterisk denotes the complex conjugate and a dot above a variable indicates time differentiation. If one uses a first-order accurate finite-difference approximation to compute the time derivatives, eq. (2) is the same as eq. (C-5) in Barnes (2007). Poggiagliolmi & Vesnaver (2014) use eq. (2) to compute the trace attributes.

### 3 THE INSTANTANEOUS QUALITY FACTOR

The IQ is defined as

$$Q_1(t) = -\pi f_1 \cdot \frac{a}{\dot{a}} = -\frac{\dot{\phi} a}{2\dot{a}} = \frac{1}{2} \cdot \frac{\Sigma_1 \dot{\Sigma}_2 - \dot{\Sigma}_1 \Sigma_2}{\Sigma_1 \dot{\Sigma}_1 + \Sigma_2 \dot{\Sigma}_2} \quad (3)$$

(Barnes 1993), where we have used eq. (2). This definition is clear in the following. Assume a simple stationary wave in a constant- $Q$  medium,

$$z = \exp(i\Omega t), \quad \Omega = \omega + i\beta, \quad (4)$$

where

$$\beta = \frac{\omega}{2Q}, \quad (5)$$

and  $Q$  is the quality factor. The amplitude and phase are then

$$a(t) = \exp(-\beta t) \quad \text{and} \quad \phi(t) = \omega t. \quad (6)$$

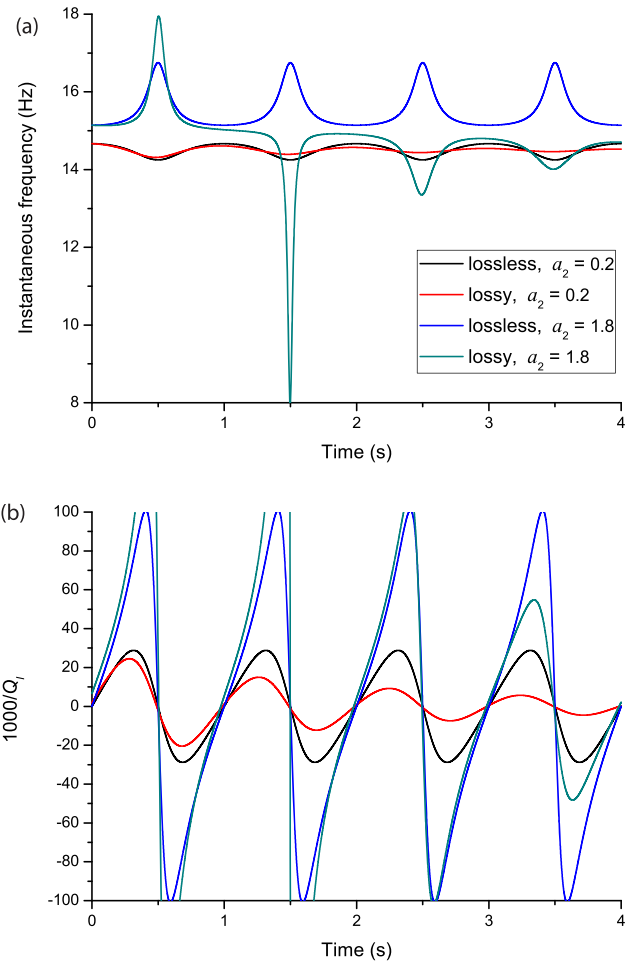


**Figure 5.** (a) IF and (b) IQ for the Mandel example in the lossless and lossy cases, where  $a_1 = 1$ ,  $Q_1 = \infty$ ,  $Q_2 = 100$ ,  $f_0 = 15$  Hz and  $\Delta f = 0.5$  Hz. The black and blue colours correspond to the lossless case, whereas the red and green colours correspond to  $a_2 = 0.2$  and 1.8, respectively.

Substituting these quantities into eqs (2) and (3) gives  $f_1 = \omega/(2\pi) = f$  and  $Q_1 = Q$ , where  $f$  is the frequency.

## 4 EXAMPLES

### 4.1 Multiple-tone signal

Let us assume a real signal  $s(t)$  composed of  $N$  harmonic frequency components (a sum of cosines),  $\omega_j, j = 1, \dots, N$ ,

$$s(t) = \sum_{j=1}^N a_j \cos(\omega_j t), \quad (7)$$

where  $\omega_j > 0$  and  $a_j$  are constant amplitudes. Its Fourier spectrum is

$$S(\omega) = \pi \sum_{j=1}^N a_j [\delta(\omega - \omega_j) + \delta(\omega + \omega_j)]. \quad (8)$$

Since the Hilbert transform of the cosine function is the sine (Bracewell & Bracewell 1986), we have

$$z(t) = \sum_{j=1}^N a_j \exp(i\omega_j t). \quad (9)$$

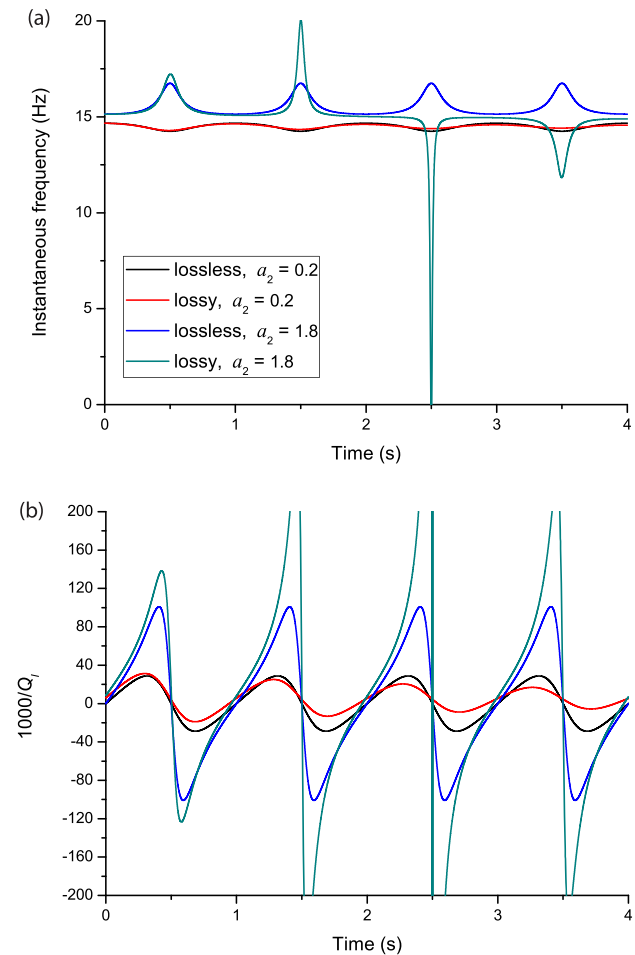


**Figure 6.** (a) IF and (b) IQ for the Mandel example in the lossless and lossy cases, where  $a_1 = 1$ ,  $Q_1 = 200$ ,  $Q_2 = 100$ ,  $f_0 = 15$  Hz and  $\Delta f = 0.5$  Hz. The black and blue colours correspond to the lossless case, whereas the red and green colours correspond to  $a_2 = 0.2$  and  $1.8$ , respectively.

The complex trace can be separated into instantaneous amplitude  $a(t)$  and phase  $\phi(t)$ , such that

$$\sum_{j=1}^N a_j \exp(i\omega_j t) = a(t) \exp[i\phi(t)], \quad (10)$$

where

$$a(t) = \sqrt{\Sigma_1^2 + \Sigma_2^2}, \quad \phi(t) = \arctan\left(\frac{\Sigma_1}{\Sigma_2}\right), \quad (11)$$

where

$$\Sigma_1 = \sum_{j=1}^N a_j \sin(\omega_j t) \quad \text{and} \quad \Sigma_2 = \sum_{j=1}^N a_j \cos(\omega_j t). \quad (12)$$

After some simple calculations, we obtain

$$f_I(t) = \frac{\cos^2 \phi}{2\pi \Sigma_2} \sum_{j=1}^N a_j \omega_j [\cos(\omega_j t) + \sin(\omega_j t) \tan \phi] \quad (13)$$

and

$$Q_I(t) = \frac{\pi f_I a^2(t)}{\sum_{j=1}^N a_j \omega_j [\Sigma_1 \cos(\omega_j t) - \Sigma_2 \sin(\omega_j t)]}. \quad (14)$$

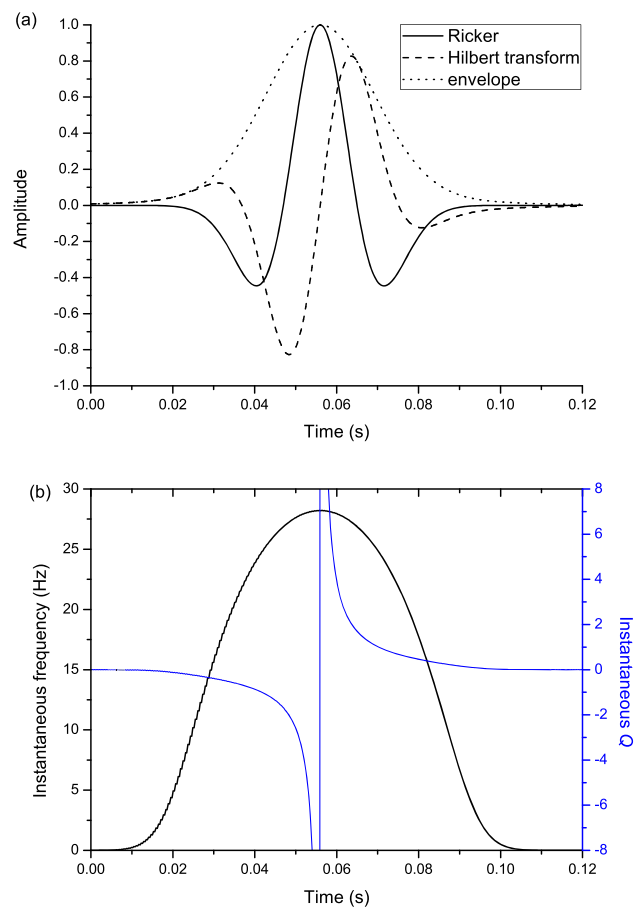


**Figure 7.** Real and imaginary parts of the complex trace (Ricker and its Hilbert transform, respectively) and trace envelope (a), and IF and IQ (b), corresponding to a Ricker wavelet of dominant frequency  $f_p = 25$  Hz. The peak IF is  $(2/\sqrt{\pi})f_p = 1.1284 f_p$ .

Let us assume that  $\omega_j$  is such that the frequency  $f = \omega/(2\pi)$  spans from 10 to 110 Hz with centre frequency at 60 Hz, and consider three amplitude distributions, that is

$$\begin{aligned} a_j &= 1, \forall j, && \text{uniform,} \\ &= \sin(0.07j), && \text{sine,} \\ &= \cos(0.07j), && \text{cosine,} \end{aligned}$$

where  $j = 1$  and  $N = 100$  correspond to 10 and 110 Hz, respectively. Fig. 1 shows the amplitude distribution  $a_j$  (a) and the IF (b) as a function of frequency and time, respectively. The uniform distribution gives an average frequency of 60 Hz, but the sine and cosine distributions show anomalous behaviours, with deviations beyond the frequency range of the signal (0–120 Hz), including negative frequencies. Then, the IF cannot be seen as the average frequency. A similar behaviour has been observed by Mandel (1974), Cohen (1995, fig. 2.2) and Loughlin & Tacer (1997) using simpler signals.

## 4.2 Mandel signal

The Mandel example is a particular case of eq. (1),

$$z(t) = a_1 \exp(i\omega_1 t) + a_2 \exp(i\omega_2 t), \quad (15)$$

where  $N = 2$  in eq. (9),  $\omega_1 = \omega_0 - \Delta\omega$  and  $\omega_2 = \omega_0 + \Delta\omega$ , with  $a_1$  and  $a_2$  constants. The IF is

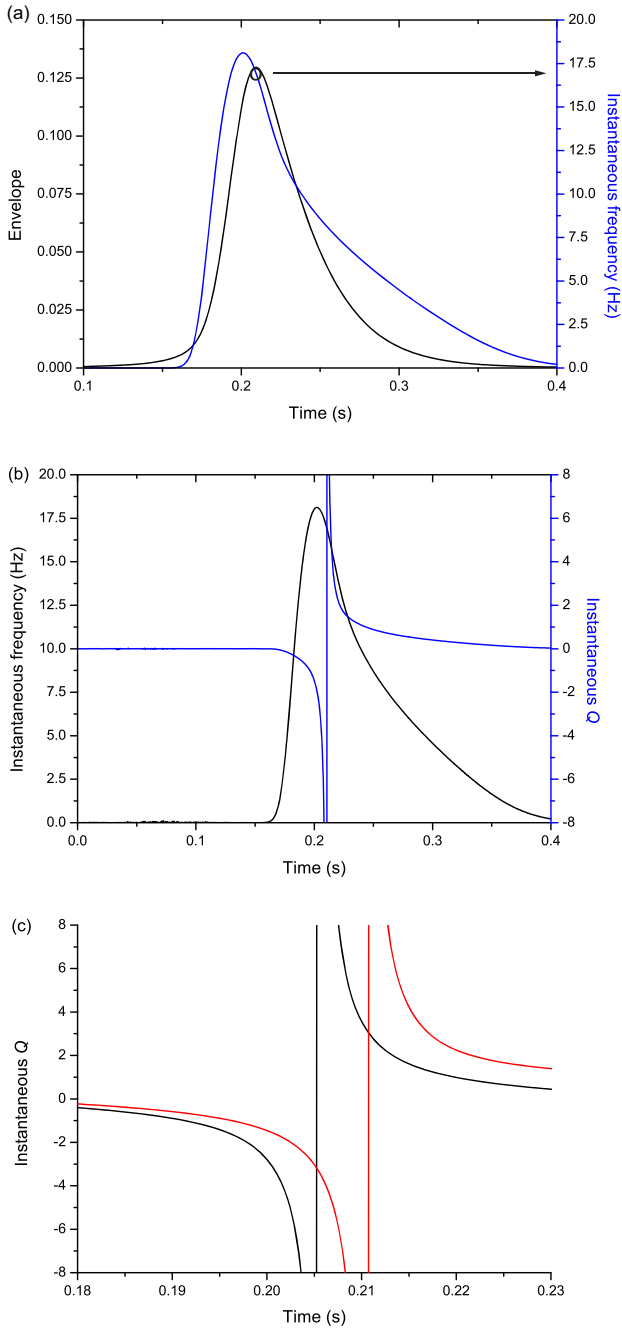


**Figure 8.** Propagation in a homogeneous medium with  $Q = 5$ . (a) Trace envelope and IF; (b) IF and IQ (b); (c) IQ (red line) compared to the lossless IQ (black line). The open circle in panel (a) indicates the IF at the peak envelope, which is the centroid frequency according to eq. (A2).

$$f_1(t) = f_0 + \frac{\Delta f(a_2^2 - a_1^2)}{a^2(t)}, \quad (16)$$

where

$$a^2(t) = \Sigma_1^2 + \Sigma_2^2 = a_1^2 + a_2^2 + 2a_1a_2 \cos(4\pi \Delta f t), \quad (17)$$

$\omega_0 = 2\pi f_0$  and  $\Delta\omega = 2\pi \Delta f$ . Cohen (1995) stated: ‘... while the IF can range widely, the occurrences when it ranges outside the bandwidth of the signal have small duration and hence do not contribute significantly ...’. Let us consider an example with  $f_0 = 15$  Hz and

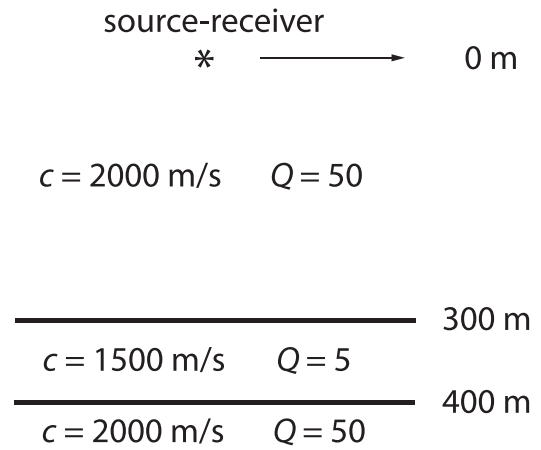


**Figure 9.** 1-D layered model to simulate wave propagation along the vertical direction.

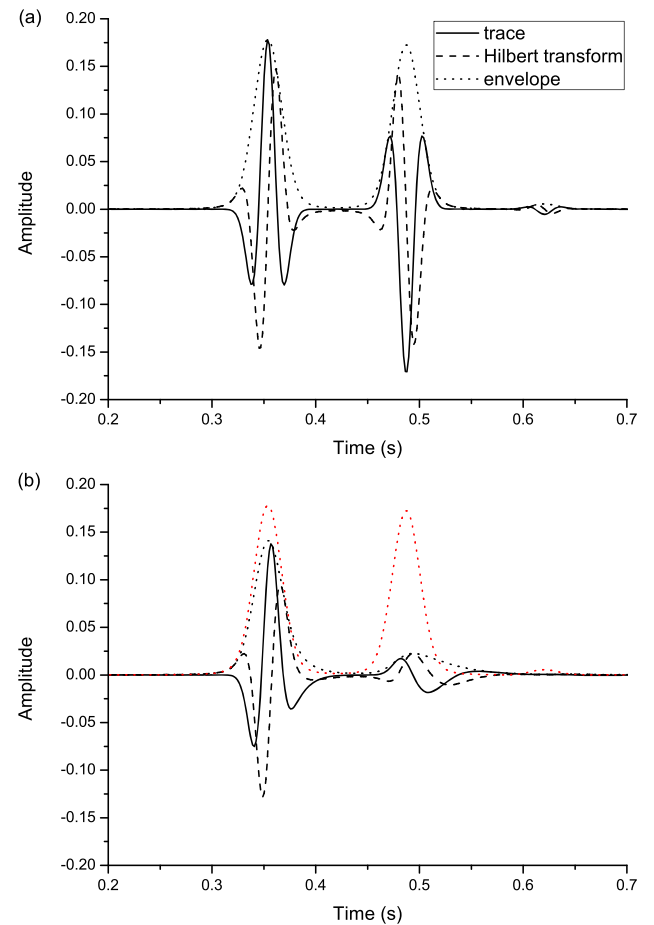


**Figure 10.** Complex-trace attributes in the (a) elastic and (b) anelastic cases. The dotted lines are the signal envelopes. The red curve in panel (b) is the envelope in the elastic case.

two different values of  $\Delta f = 5$  and  $0.5$  Hz. Based on eq. (16), Fig. 2 shows that the contributions have components outside the band of the signal:  $[10, 20]$  Hz in (a) and  $[15.5, 14.5]$  Hz in (b), even for moderate signal durations. The IF shows a physical behaviour when their averages and peak values are computed. This is illustrated in

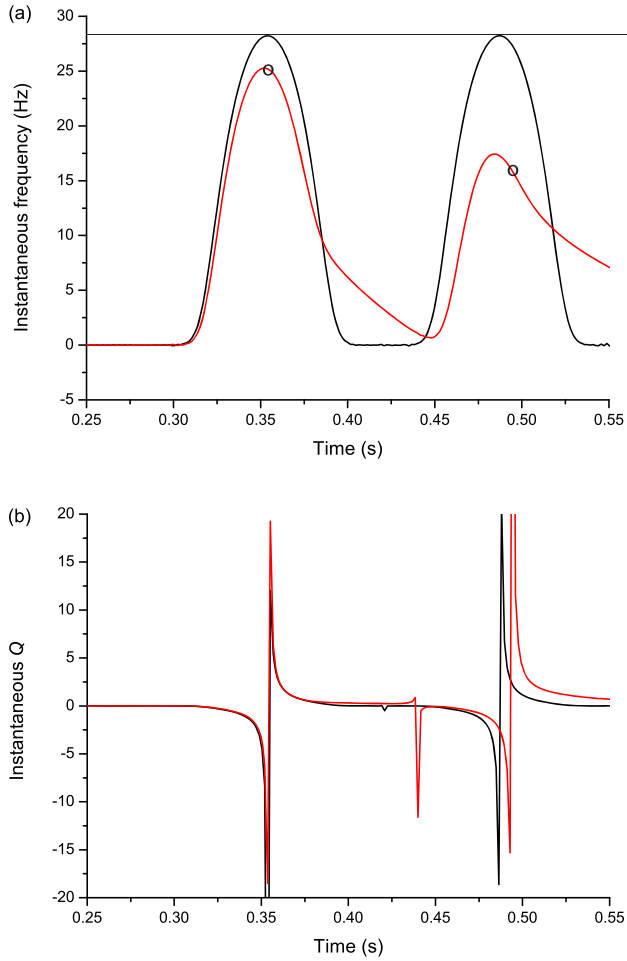


**Figure 11.** (a) IF and (b) IQ corresponding to the signals of Fig. 8, where the black and red lines correspond to the lossless (elastic) and lossy (anelastic) cases, respectively. The horizontal line refers to 28.2 Hz, while the open circles refer to  $\langle f \rangle_2$ .

Appendix A, where it is shown that the centroid of the energy spectrum equals the average IF and the centroid of the spectrum equals the IF evaluated at the peak of the signal envelope  $a(t)$ . On the other hand, the IQ is

$$Q_1(t) = \frac{f_1 a^2(t)}{4a_1 a_2 \Delta f \sin(4\pi \Delta f t)} = \frac{a_2^2 - a_1^2 + (f_0/\Delta f) a^2(t)}{4a_1 a_2 \sin(4\pi \Delta f t)}. \quad (18)$$

It is clear that the wave (eq. 15) is not subject to intrinsic loss, since the  $\omega_j$  are real quantities, and therefore the wave is not damped. However, Fig. 3 shows that the inverse of the IQ takes values other than zero, including negative values, although oscillates around a zero mean value, since the time average of  $Q_1^{-1}$  has the form

$$\int Q_1^{-1}(t) dt \propto \ln[A + B \cos(4\pi \Delta f t)], \quad (19)$$

where  $A$  and  $B$  are constants (Jeffrey & Zwillinger 2007, p. 172, eq. 2.553). Since the integral is an even function, the mean value is zero.

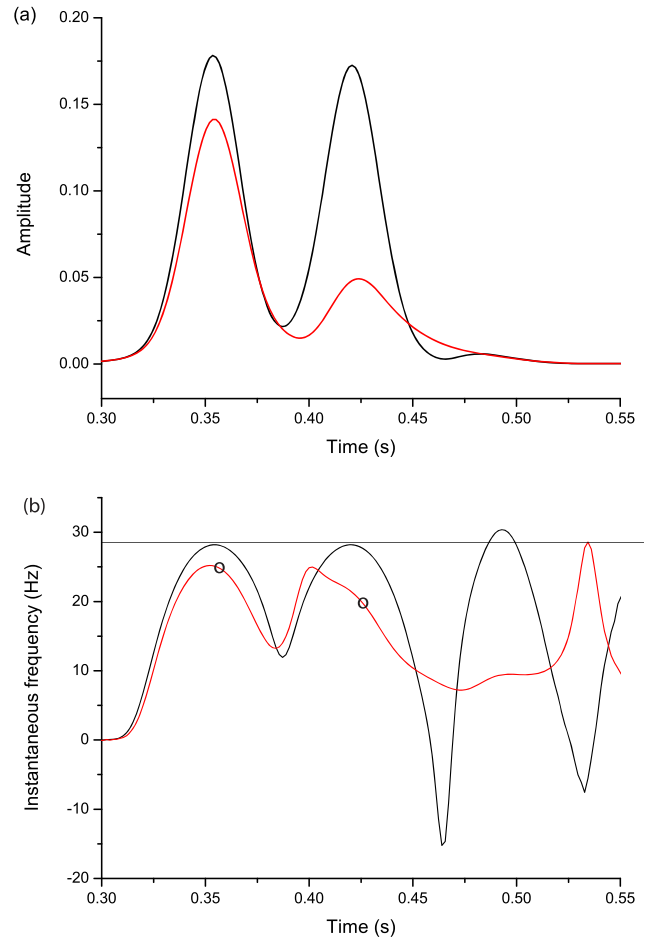


**Figure 12.** (a) Envelope and (b) IF in the elastic (black line) and anelastic (red line) cases, where the layer thickness is 50 m. The horizontal line refers to 28.2 Hz, the Ricker's centroid frequency, and the open circles refer to values of  $\langle f \rangle_2$ .

### 4.3 Generalization of the Mandel signal

Let us now consider the generalization of the Mandel example to the lossy case,

$$z(t) = a_1 \exp(i\Omega_1 t) + a_2 \exp(i\Omega_2 t), \quad \Omega_i = \omega_i + i s \beta_i, \quad (20)$$

where  $s = \text{sgn}(t)$ ,

$$\beta_i = \frac{\omega_i}{2Q_i}, \quad i = 1, 2, \quad (21)$$

in agreement with eq. (5).  $z(t)$  is a damped stationary wave and the sign function is included to have damping also from  $t = -\infty$  to 0. Apparently, this signal has no relation to the seismic case. It is however a simple combination of exponential functions with different frequencies and therefore a simplified version of a real seismic signal (e.g. Tary *et al.* 2014, eq. 10). Moreover, the objective here is to study the effect of attenuation on the IQ.

In this case,

$$\begin{aligned} \Sigma_1 &= \text{Im}(z) = \gamma_1 \sin(\omega_1 t) + \gamma_2 \sin(\omega_2 t), \\ \Sigma_2 &= \text{Re}(z) = \gamma_1 \cos(\omega_1 t) + \gamma_2 \cos(\omega_2 t), \\ a^2(t) &= \Sigma_1^2 + \Sigma_2^2 = \gamma_1^2 + \gamma_2^2 + 2\gamma_1 \gamma_2 \cos(4\pi \Delta f t), \\ \gamma_i(t) &= a_i \exp(-\beta_i |t|), \end{aligned} \quad (22)$$

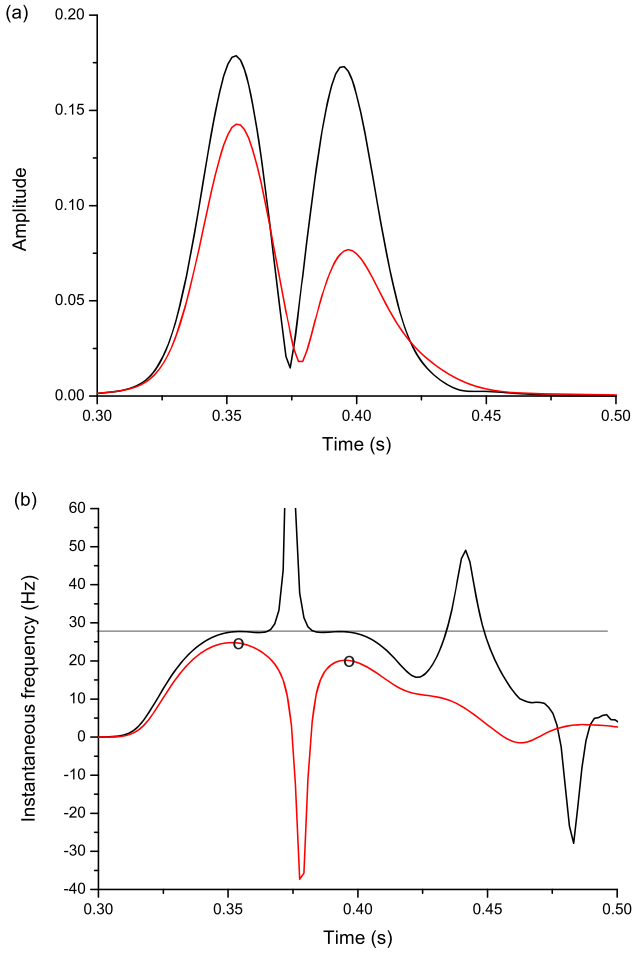


Figure 13. As Fig. 11, but the layer thickness is 30 m.

where  $\omega_1 = 2\pi(f_0 - \Delta f)$ ,  $\omega_2 = 2\pi(f_0 + \Delta f)$ , with  $f_0 = (\omega_1 + \omega_2)/(4\pi)$ . To compute the phase, which has the form (11), it is simpler to differentiate the complex quantities and then take the real part. We then obtain the IF from eq. (2), where

$$\begin{aligned} \dot{\Sigma}_1 &= \gamma_1[\omega_1 \cos(\omega_1 t) - s\beta_1 \sin(\omega_1 t)] \\ &\quad + \gamma_2[\omega_2 \cos(\omega_2 t) - s\beta_2 \sin(\omega_2 t)], \\ -\dot{\Sigma}_2 &= \gamma_1[\omega_1 \sin(\omega_1 t) + s\beta_1 \cos(\omega_1 t)] \\ &\quad + \gamma_2[\omega_2 \sin(\omega_2 t) + s\beta_2 \cos(\omega_2 t)], \end{aligned} \quad (23)$$

where we have used the property  $d|t|/dt = t/|t| = s$ . On the other hand, the IQ is given by eq. (3).

Let us first consider  $Q_1 = Q_2 = 30$ . Fig. 4 shows the IF (a) and IQ (b) as a function of time compared to the lossless case. A slight damping as a function of time is observed for  $a_2 = 0.2$ , but the IF is amplified for  $a_2 = 1.8$ . The mean value of the IQ is 30 (e.g. the red and green curves are shifted upwards). Fig. 5 shows a similar plot with  $Q_1 = \infty$  and  $Q_2 = 100$ . A strong damping of the IF can be seen for  $a_2 = 0.2$ , and the trend is inverted from the second peak for  $a_2 = 1.8$ . The case  $Q_1 = 200$  and  $Q_2 = 100$  is displayed in Fig. 6, where it can be seen that the IF reaches the zero value and the inverse IQ takes very high values (strong attenuation).

#### 4.4 Ricker wavelet-based trace

A more realistic geophysical signal is based on a source given by the Ricker wavelet, whose expression is

$$s(t) = (1 - 2a^2) \exp(-a^2), \quad a = \pi f_p(t - t_s), \quad (24)$$

where  $f_p$  is peak frequency and we take  $t_s = 1.4/f_p$ . Its frequency spectrum is

$$S(\omega) = \frac{2\bar{a}^2}{\sqrt{\pi} f_p} \exp(-\bar{a}^2 - i\omega t_s), \quad \bar{a} = \frac{\omega}{\omega_p} = \frac{f}{f_p}. \quad (25)$$

Denoting by  $\mathcal{F}$  and  $\mathcal{F}^{-1}$  the forward and inverse Fourier operators, the complex trace is

$$z(t) = \mathcal{F}^{-1}[Z(\omega)], \quad Z(\omega) = \begin{cases} V(\omega), & \omega = 0, \\ 2V(\omega), & \omega > 0, \\ 0, & \omega < 0, \end{cases} \quad (26)$$

where  $V$  is the spectrum of the trace (Cohen 1995, p. 30). The real part of  $z(t)$  is  $v(t) = s(t)$  and the imaginary part is the Hilbert transform of  $v(t)$ .

The IF and IQ are given by eqs (2) and (3), where

$$\Sigma_1 = \text{Im}(z), \quad \Sigma_2 = \text{Re}(z), \quad \dot{\Sigma}_1 = \text{Im}(\dot{z}), \quad \dot{\Sigma}_2 = \text{Re}(\dot{z}). \quad (27)$$

We compute the time derivatives with the Fourier pseudo-spectral method. For instance,  $\Sigma_2 = u(t) \xrightarrow{\text{FFT}} U(\omega) \rightarrow i\omega U(\omega) \xrightarrow{\text{FFT}^{-1}} \dot{u}(t) = \dot{\Sigma}_2$ , where FFT is the fast Fourier transform (e.g. Carcione, 2014, Section 9.9.5). From eq. (2),  $f_I = \text{Re}[\dot{z}/(2\pi iz)]$ , so that

$$f_I = \frac{1}{2\pi} \text{Im} \left[ \frac{\dot{z}}{z} \right], \quad (28)$$

constituting an alternative test. In particular, the length of the FFT in these computations is  $2^9 = 512$  and the time step for the discretization is  $dt = 1.6$  ms. First, we consider the Ricker wavelet  $v(t) = s(t)$  with  $f_p = 25$  Hz. Robertson & Nogami (1984) showed explicitly that the IF computed at the time corresponding to the peak of the envelope is  $f_I = (2/\sqrt{\pi})f_p = 1.1284 \times f_p = 28.2095$  Hz, and it is equal to the spectrum centroid  $\langle f \rangle_2$ , in agreement with eq. (A2). This is shown in Fig. 7 together with the complex-trace properties, where in particular, the IQ takes very low positive and negative non-zero values and tends to high values at the signal peak. Moreover, eq. (A1) yields  $\langle f \rangle_1 = 26.5961$  Hz. Next, we compute synthetic seismograms with the modelling method outlined in Appendix B. The source peak frequency is  $f_p = 25$  Hz. The grid spacing is 1 m and the time step is 0.1 ms, resampled to 0.4 ms to obtain a time-series of  $2^{11} = 2048$  samples (maximum time is 0.8192 s). First, we consider a homogeneous medium and propagation from source to a receiver located at 300 m (the velocity  $c$  equal to  $2 \text{ km s}^{-1}$  and the density is  $1741 \text{ kg m}^{-3}$ ). For  $Q = \infty$ , the results are similar to those of Fig. 7, since in this case, the signal propagates without attenuation and velocity dispersion. The results for  $Q = 5$  are shown in Fig. 8. The open circle in (a) indicates the IF at the peak envelope, which is the centroid frequency according to eq. (A2). This frequency decreases from 28.20 Hz to approximately 16.5 Hz. The IQ has the same features as in the lossless case; the only difference is a shift of the singularity (5 ms), related to the velocity dispersion. Next, we consider the model shown in Fig. 9, consisting of a layer of thickness 100 m with velocity  $c = 1.5 \text{ km s}^{-1}$  and  $Q = 5$  embedded in a homogeneous medium characterized by  $c = 2 \text{ km s}^{-1}$  and  $Q = 50$ . The densities of the two media are  $1741 \text{ kg m}^{-3}$ . The source coincides with the receiver and is located 300 m above the layer. Fig. 10 shows the complex trace, with (a) and (b) corresponding to the lossless (elastic) and lossy (anelastic) cases, respectively. The direct wave

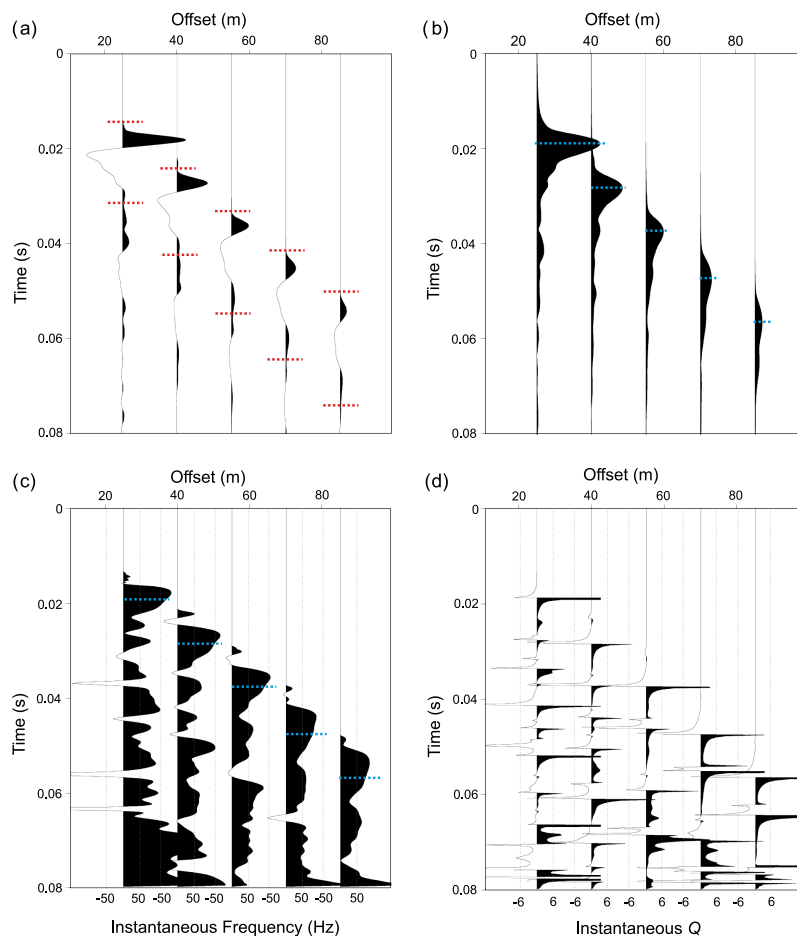


**Figure 14.** (a) Hammer shallow-refraction seismogram as recorded on the horizontal transverse component ( $SH$  waves). The red dashed lines indicate the time windows used for the Fourier transform of the first-break wavelets. (b) Envelope and (c) IF of the seismograms, where the blue dashed lines refer to the traveltimes at the envelope peaks. (d) IQ of the recorded signals.

(at  $t = 0$ ) is filtered by applying to the seismograms a cosine taper preserving the reflection response of the layer. A strong damping is observed in (b), as well as velocity dispersion if one compares the envelopes (red and black dotted lines in Fig. 10b). The envelopes have peaks at the two reflection events corresponding to the upper and lower interface of the layer. The propagation times: 0.3536 and 0.4780 s (lossless case) and 0.3551 and 0.4944 s (lossy case). Fig. 11 shows the IF and IQ in a time window that includes the two events. The IF at the peak envelope in the lossless case is 28.2 Hz for both events as expected, while the IFs in the lossy case are 25.1 and 15.91 Hz, which should correspond to the centroid frequencies given by eq. (A2). Eq. (A1) yields  $\langle f \rangle_1 = 26.61$  Hz and 13.54 Hz in the lossless and lossy cases, respectively. The IQ (Fig. 11b) shows negative values and the behaviour is not very dissimilar to that of the elastic case, so that no useful information can be inferred. The shift around 0.5 s is due to the dispersion effect of anelasticity, since the pulse in the lossy case is slower. We recall that dispersion in this case means that each frequency component of the signal travels with a different velocity and since the lossless (elastic) case is defined at the high frequencies (or instantaneous response in the time domain), the overall effect of anelasticity is to delay the signal. Figs 12 and 13 show the envelopes and IFs in the elastic (black line) and anelastic (red line) cases, for layer thicknesses of 50 m and 30 m, respectively. The two events overlap but the envelope peaks can be discriminated. The horizontal lines indicate the centroid frequency

of the Ricker wavelet, which coincides with the IF at the peak of the two events in the lossless case. These values can be used to compute the frequency shift required by the tomography methods (Quan & Harris 1997) (see Figs 12b and 13b). The IF can take positive and negative high values away from the envelope peaks, as can be seen in Fig. 13(b), which shows a situation similar to that of fig. 5a in Barnes (1993). These high values have also been predicted by Robertson & Nogami (1984), when the layer thickness are about a quarter period of the signal and remains high as the layer continues to thin. These spike-like features occur at envelope minima and are numerical artefacts due to a numerical instability when computing the time derivatives or due to zeroes in the denominator in eq. (2), which have to be filtered as in Yedlin *et al.* (2013).

Adding random noise could, in principle, worsen the interpretation, but when dealing with signal processing methods and attribute analysis, it is known that noise (nearly white) most of the times ‘helps’ summations and divisions, at areas where the signal amplitude is zero (or at local maxima or minima), creating instabilities. However, we cannot rely on this fact and it is reasonable to state that if an algorithm does not work with synthetic (well-controlled) data, its application to real data cannot be better. The effect of noise can be reduced by smoothing the frequency-time data, but reducing both time and frequency resolution. Moreover, IF analysis also relies on the use of specific filtering methods (e.g. Wiener), and can be relatively intensive computationally. A relevant analysis of the

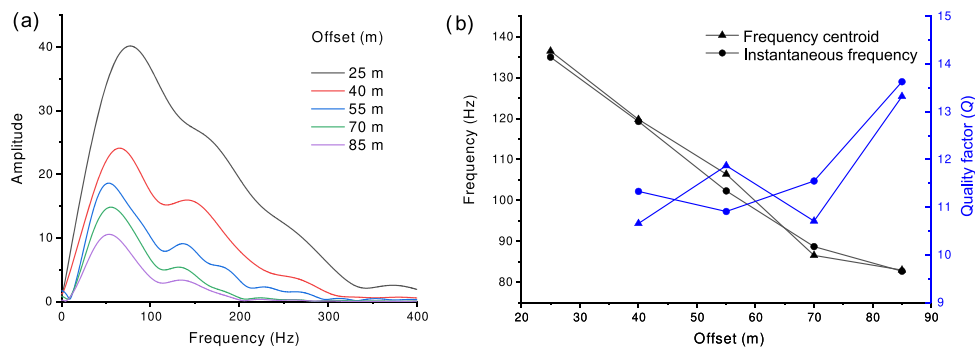


**Figure 15.** (a) Amplitude spectra of the wavelets selected from the seismograms of Fig. 14(a). (b) Comparison between the spectral centroids and the IFs selected at the envelope peaks, as shown in Fig. 14(c), and corresponding quality factors computed with the frequency-shift method.

performance of IF analysis is performed in Reiz & Morgos (2013) and Xing *et al.* (2019), while Tary *et al.* (2014) review several types of spectral estimations other than IF.

#### 4.5 Analysis of real seismic data

We consider an application to real seismic data acquired on the Pian di Neve glacier (Adamello massif, Italian Alps) by Picotti *et al.* (2017) to assess the firn and ice seismic properties. Both *P* and *S* waves were propagated in the subsurface by hammering on a wooden plate embedded in the snow. The data were acquired using a 24-channel seismic recording system with 10 Hz vertical and horizontal geophones regularly spaced at 5 m. We consider five traces, 15 m spaced, from the seismogram shown in Fig. 2(a) in that paper. We select the *SH*-wave first breaks refracted at the base of the firn and recorded between 25 and 85 m offset (Fig. 14a). We estimate the *SH*-wave *Q* factor of the ice below the shallow firn layer by using the frequency-shift method (Quan & Harris 1997) applied to the wavelet centroid frequencies and the IF peaks. Fig. 15(a) shows the amplitude spectra of the wavelets selected from the seismograms (see the time windows in Fig. 14a). The maximum useful signal frequency being about 350 Hz, we apply a low-pass filter to eliminate the high-frequency random noise and stabilize the first-derivative computation. Fig. 14 displays the envelope (b), IF (c) and IQ (d) of the signals represented in panel (a). Fig. 15(b) shows the comparison between the spectral centroids and the IFs evaluated at the envelope peaks (blue dashed lines in Fig. 14b) and between the corresponding *Q* factors. The frequency-shift computation has been done considering as reference signal the (first) wavelet recorded at 25 m offset and an *SH*-wave velocity of  $1750 \text{ m s}^{-1}$ , obtained from the first-break traveltimes. The agreement between frequencies and *Q* factors is very good, while the IQ represented in Fig. 14(d) does not add any useful new information to this analysis. The *Q* factor values range between 10 and 14, denoting the presence of a highly attenuating medium, the medium being just below the firn not pure ice. This fact is also confirmed by the *SH*-wave velocity value, which is lower than that of pure ice ( $1860 \text{ m s}^{-1}$ ) inferred from the far-offset first breaks of the same data set.

## 5 CONCLUSIONS

We have analysed the IF and IQ of a two-tone stationary and lossy signal, showing that these concepts cannot be interpreted as physical averages as a function of time, since the IF may fall outside the range of frequencies of the signal, and the IQ takes non-zero values in the

lossless case, and can take very high positive and negative values in the lossy case. The correct interpretation of the IF involves averages and specific values at fixed times, which coincide with the centroids of the signal spectrum. However, using IF to establish the presence of hydrocarbon-saturated rocks on the basis of low-frequency shadows is dubious, since low frequencies may be due to other causes, such as unphysical low values of this attribute, NMO stretch, which is important at far offset traces, etc. Basically, complex seismic-trace analysis provides the same information as the Fourier analysis, which produces global measures. Unlike spectrograms, IF cannot be interpreted as the average frequency at each time in the signal, and IQ only reveals the degree of velocity dispersion. However, the complex-trace attributes, specifically IF, at the maximum of instantaneous amplitude in an event (signal envelope) can be used instead of the Fourier transform to estimate dominant frequency changes with time, avoiding, in theory, the subjective use of time windows. Ideally, events have to correspond to single interfaces, since interference can generate false interpretations, and the signal-to-noise ratio has to be high enough. An example of application to real seismic data is shown. Thus, despite the amount of literature published on the subject, IF and IQ are of limited use from a practical point of view, and a misuse can lead to erroneous interpretations. In summary, although the novel aspect in this work regards the IQ, alternative examples of the IF are given, considering signals that can lead to false interpretations. Some of these cases were not considered in the geophysical literature.

## DATA AVAILABILITY

The data underlying this paper will be shared on request to the corresponding author.

## REFERENCES

- Ba, J., Zhao, J., Carcione, J.M. & Huang, X., 2016. Compressional wave dispersion due to rock matrix stiffening by clay squirt flow, *Geophys. Res. Lett.*, **43**(12), 6186–6195.
- Ba, J., Ma, R., Carcione, J.M. & Picotti, S., 2019. Ultrasonic wave attenuation dependence on saturation in tight oil siltstones, *J. Pet. Sci. Eng.*, **179**, 1114–1122.
- Barnes, A.E., 1991. Instantaneous frequency and amplitude at the envelope peak of a constant-phase wavelet, *Geophysics*, **56**(7), 1058–1060.
- Barnes, A.E., 1993. Instantaneous spectral bandwidth and dominant frequency with applications to seismic reflection data, *Geophysics*, **58**(3), 419–428.
- Barnes, A.E., 2007. A tutorial on complex seismic trace analysis, *Geophysics*, **72**(6), W33–W43.

- Barnes, A.E., 2013. The myth of low frequency shadows, in *EAGE Workshop on Seismic Attenuation*, cp-363, European Association of Geoscientists & Engineers, Singapore.
- Boashash, B., 1992. Estimating and interpreting the instantaneous frequency of a signal. I. Fundamentals, *Proc. IEEE*, **80**(4), 520–538.
- Bracewell, R.N. & Bracewell, R.N., 1986. *The Fourier Transform and Its Applications*, McGraw-Hill.
- Carcione, J.M., 2014. *Wave Fields in Real Media: Wave Propagation in Anisotropic, Anelastic, Porous and Electromagnetic Media*, 3rd edn, Elsevier Science.
- Carcione, J.M., Qadrouh, A.N., Perroud, H., Gei, D., Ba, J. & Picotti, S., 2018. Seismic attenuation, normal moveout stretch, and low-frequency shadows underlying bottom simulating reflector events, *Geophys. Prospect.*, **66**(5), 857–871.
- Castagna, J.P., Sun, S. & Siegfried, R.W., 2003. Instantaneous spectral analysis: detection of low-frequency shadows associated with hydrocarbons, *Leading Edge*, **22**(2), 120–127.
- Cohen, L., 1995. *Time-Frequency Analysis*, Vol. 778, Prentice Hall.
- Ebrom, D., 2004. The low-frequency gas shadow on seismic sections, *Leading Edge*, **23**(8), 772.
- Engelhard, L., 1996. Determination of seismic-wave attenuation by complex trace analysis, *Geophys. J. Int.*, **125**(2), 608–622.
- Fischer, J.V. A Paradox of Unity. Preprints 2018, doi: 10.20944/preprints201801.0003.v1.
- Gabor, D., 1946. Theory of communication, *J. Inst. Electr. Eng.*, **93**, 429–457.
- Gao, J., Yang, S., Wang, D. & Wu, R., 2011. Estimation of quality factor  $Q$  from the instantaneous frequency at the envelope peak of a seismic signal, *J. Comput. Acoust.*, **19**(02), 155–179.
- Geletti, R. & Busetti, M., 2011. A double bottom simulating reflector in the western ross sea, Antarctica, *J. geophys. Res.*, **116**(B4), doi:10.1029/2010JB007864.
- Jeffrey, A. & Zwillinger, D., 2007. *Table of Integrals, Series, and Products*, Elsevier.
- Lin, R., Vesnaver, A., Böhm, G. & Carcione, J., 2018. Broad-band viscoacoustic  $Q$ -factor imaging by seismic tomography and instantaneous frequency, *Geophys. J. Int.*, **214**(1), 672–686.
- Loughlin, P.J. & Tacer, B., 1997. Comments on the interpretation of instantaneous frequency, *IEEE Signal Process. Lett.*, **4**(5), 123–125.
- Mandel, L., 1974. Interpretation of instantaneous frequencies, *Am. J. Phys.*, **42**(10), 840–846.
- Marfurt, K. & Kirlin, R., 2001. Narrow-band spectral analysis and thin-bed tuning, *Geophysics*, **66**(4), 1274–1283.
- Matheny, M.P. & Nowack, R.L., 1995. Seismic attenuation values obtained from instantaneous-frequency matching and spectral ratios, *Geophys. J. Int.*, **123**(1), 1–15.
- Pang, M., Ba, J., Carcione, J.M., Picotti, S., Zhou, J. & Jiang, R., 2019. Estimation of porosity and fluid saturation in carbonates from rock-physics templates based on seismic  $Q$ , *Geophysics*, **84**(6), M25–M36.
- Picotti, S., Francese, R., Giorgi, M., Pettenati, F. & Carcione, J.M., 2017. Estimation of glacier thicknesses and basal properties using the horizontal-to-vertical component spectral ratio (HVSr) technique from passive seismic data, *J. Glaciol.*, **63**(238), 229–248.
- Poggiagliolmi, E. & Vesnaver, A., 2014. Instantaneous phase and frequency derived without user-defined parameters, *Geophys. J. Int.*, **199**(3), 1544–1553.
- Qadrouh, A.N., Carcione, J.M., Salim, A.M. & Harith, Z.Z.T., 2016. Seismic spectrograms of an anelastic layer with different source-receivers configurations, *Arab. J. Geosci.*, **9**(5), 413, doi:10.1007/s12517-016-2429-3.
- Quan, Y. & Harris, J.M., 1997. Seismic attenuation tomography using the frequency shift method, *Geophysics*, **62**(3), 895–905.
- Reiz, R. & Morgos, L., 2013. IF estimation using spectrogram and scalogram, *J. Electr. Electron. Eng.*, **6**(2), 25.
- Robertson, J.D. & Nogami, H.H., 1984. Complex seismic trace analysis of thin beds, *Geophysics*, **49**(4), 344–352.
- Saha, J., 1987. Relationship between Fourier and instantaneous frequency, in *SEG Technical Program Expanded Abstracts 1987*, pp. 591–594, Society of Exploration Geophysicists.
- Sinha, S., Routh, P.S., Anno, P.D. & Castagna, J.P., 2005. Spectral decomposition of seismic data with continuous-wavelet transform, *Geophysics*, **70**(6), P19–P25.
- Taner, M.T., Koehler, F. & Sheriff, R., 1979. Complex seismic trace analysis, *Geophysics*, **44**(6), 1041–1063.
- Tary, J.B., Herrera, R.H., Han, J. & van der Baan, M., 2014. Spectral estimation—what is new? what is next? *Rev. Geophys.*, **52**(4), 723–749.
- Tonn, R., 1991. The determination of the seismic quality factor  $Q$  from VSP data: a comparison of different computational methods, *Geophys. Prospect.*, **39**(1), 1–27.
- Wang, Z., Gao, J., Zhou, Q., Li, K. & Peng, J., 2013. A new extension of seismic instantaneous frequency using a fractional time derivative, *J. Appl. Geophys.*, **98**, 176–181.
- Xing, L., Aarre, V., Barnes, A.E., Theoharis, T., Salman, N. & Tjåland, E., 2019. Seismic attribute benchmarking on instantaneous frequency, *Geophysics*, **84**(3), O63–O72.
- Yang, S. & Gao, J., 2009. Seismic attenuation tomography by envelope peak instantaneous frequency, *IEEE Geosci. Remote Sens. Lett.*, **6**(3), 514–518.
- Yedlin, M.J., Margrave, G.F. & Horin, Y.B., 2013. Instantaneous frequency computation: theory and practice, in *CREWES Research Report*, Vol. 25.

## APPENDIX A: LINK BETWEEN THE AVERAGE AND PEAK IF AND CENTROID FREQUENCIES

Gabor (1946) showed that the centroid of the signal energy of the spectrum is equal to the time average of the IF,

$$\langle f \rangle_1 = \frac{\int f |Z(f)|^2 df}{\int |Z(f)|^2 df} = \frac{\int f |z(t)|^2 dt}{\int |z(t)|^2 dt} = \langle f_1 \rangle, \quad (\text{A1})$$

where  $Z(f)$  is the Fourier transform of  $z(t)$  and the integration on the spectrum is, in principle, intended from 0 to  $\infty$  if the signal is causal (see also Barnes 1993).

On the other hand, Robertson & Nogami (1984), Saha (1987) and Barnes (1991) showed that the centroid of the signal spectrum is equal to the IF at the peak of the signal envelope,

$$\langle f \rangle_2 = \frac{\int f |Z(f)| df}{\int |Z(f)| df} = f_1(t_0), \quad (\text{A2})$$

where  $t_0$  is obtained from  $\dot{a}(t = t_0) = 0$ . (Proof: For  $z$  given by eq. (10), and imposing  $\dot{a} = 0$ , it is  $\dot{z} = i\dot{\phi}z$  or  $\dot{\phi} = \dot{z}/(iz)$ ; since the Fourier transform of  $\dot{z}$  is  $2\pi i f Z(f)$ , we obtain (A2) if  $t_0$  is taken as the origin of time.) Eq. (A2) is the basis of the phase-shift method of Quan & Harris (1997) to obtain the quality factor  $Q$  (e.g. Lin et al. 2018). For instance, for a spectrum of rectangular shape of width  $W$ , it is

$$\langle f \rangle_2(\text{receiver}) \approx \langle f \rangle_2(\text{source}) - \frac{\pi W^2}{12} \cdot \frac{\tau}{Q} \quad (\text{A3})$$

(Quan & Harris 1997), where  $\tau$  is the traveltime between source and receiver. Similarly, Yang & Gao (2009) and Gao et al. (2011) obtain  $\langle f \rangle_2(\text{receiver}) \approx \langle f \rangle_2(\text{source}) - k(\tau/Q)$ , for a realistic source wavelet, where  $k$  is a constant depending on the source parameters. For  $\tau = 0$  or  $Q = \infty$ , the source and receiver centroids are the same.

Examples: Let us consider the Mandel signal (15), whose Fourier transform is

$$Z(f) = a_1 \delta(f - f_1) + a_2 \delta(f - f_2) \quad (\text{A4})$$

where  $\delta$  is Dirac delta, and

$$|z(t)|^2 = a^2(t). \quad (\text{A5})$$

(see eq. 17).

Integrating from  $-T$  to  $T$ , eq. (A1) gives

$$\langle f_I \rangle = f_0 + \frac{T \Delta f (a_2^2 - a_1^2)}{T(a_1^2 + a_2^2) + a_1 a_2 \frac{\sin(4\pi \Delta f T)}{2\pi \Delta f}}. \quad (\text{A6})$$

For  $T \rightarrow \infty$ , we obtain

$$\langle f_I \rangle = f_0 + \frac{a_2^2 - a_1^2}{a_1^2 + a_2^2} \Delta f = \langle f \rangle_1. \quad (\text{A7})$$

The second equality uses the fact that any power of the Dirac delta gives the delta (Fischer 2018).

Regarding the value of  $t$  at the maximum amplitude  $a(t)$ , it is  $\dot{a}^2 = -8a_1 a_2 \pi \Delta f \sin(4\pi \Delta f t)$  and  $\ddot{a}^2 = -32a_1 a_2 \pi^2 \Delta f^2 \cos(4\pi \Delta f t)$ . We have a maximum if the second derivative is negative. Then,  $t_0 = n/(2\Delta f)$ ,  $n = 0, 1, 2, \dots$  for  $a_1 a_2 > 0$  and  $t_0 = [n/(4\Delta f)]$ ,  $n = 1, 3, \dots$  for  $a_1 a_2 < 0$ . It is enough to take  $t_0 = 1$  and  $t_0 = 1/(4\Delta f)$ , respectively. Referring to eq. (16),  $a^2 = (a_1 + a_2)^2$  for  $a_1 a_2 > 0$  and  $a^2 = (a_1 - a_2)^2$  for  $a_1 a_2 < 0$ . Then,

$$\begin{aligned} \langle f \rangle_2 &= f_1(t_0) = f_0 + \frac{a_2 - a_1}{a_1 + a_2} \Delta f, \quad a_1 a_2 > 0, \\ \langle f \rangle_2 &= f_1(t_0) = f_0 - \frac{a_2 + a_1}{a_1 - a_2} \Delta f, \quad a_1 a_2 < 0. \end{aligned} \quad (\text{A8})$$

Assuming, without loss in generality, that  $a_1 > 0$ , the two eq. (A8) are identical.

Then,  $t_0 = 0$  for  $a_1 a_2 > 0$  and  $t_0 = 1/(4\Delta f)$  for  $a_1 a_2 < 0$ , where  $t_0$  is the time at which the signal envelope is maximum. These values are exact for the lossless case, while the second one is an approximation for the lossy case. Taking  $t_0 = 0$ , the IF in eq. (2) (peak IF) is that of the lossless case, that is eq. (A8). The Fourier transform of the lossy signal (20) is

$$Z(\omega) = \frac{2a_1 \beta_1}{\beta_1^2 + (\omega - \omega_1)^2} + \frac{2a_2 \beta_2}{\beta_2^2 + (\omega - \omega_2)^2}. \quad (\text{A9})$$

It can be shown that the centroid (A2) yields the value (A8) after performing the integrations in the numerator and denominator.

Similarly, for  $t_0 = 0$ , the IQ in eq. (3) is

$$Q_1 = \frac{(a_1 + a_2)f_0 + (a_2 - a_1)\Delta f}{(a_1 Q_1^{-1} + a_2 Q_2^{-1})f_0 + (a_2 Q_2^{-1} - a_1 Q_1^{-1})\Delta f}. \quad (\text{A10})$$

For  $Q_1 = Q_2 = Q_0$ , we obtain  $Q_1 = Q_0$ .

## APPENDIX B: FULL-WAVEFORM MODELLING METHOD

The full-waveform synthetic seismograms are computed with a modelling code based on the viscoacoustic stress–strain relation corresponding to a single relaxation mechanism, represented by the Zener or standard-linear-solid mechanical model. The equations are given in Section 2.10.4 of Carcione (2014). The 1-D particle velocity–stress formulation describing propagation along the  $x$ -direction is

$$\begin{aligned} \dot{v} &= \frac{1}{\rho} \partial_x \sigma, \\ \dot{\sigma} &= \rho c^2 (\partial_x v + e) + s, \\ \dot{e} + \frac{e}{\tau_\sigma} + \left( \frac{2}{\tau_\sigma Q} \right) \partial_x v &= 0, \end{aligned} \quad (\text{B1})$$

where  $v$  is particle velocity,  $\sigma$  is stress,  $s$  is the source (explosion),  $e$  is a memory variable,  $\tau_\sigma$  denotes a relaxation time and a dot above a variable indicates time differentiation. The relaxation time is

$$\tau_\sigma = \tau_0 \left( \sqrt{Q^{-2} + 1} - Q^{-1} \right), \quad (\text{B2})$$

where  $Q$  is the minimum quality factor and  $\tau_0 = 1/2\pi f_0$ . If  $f_p$  is the central frequency of the source wavelet, we assume that the relaxation peak is located at  $\omega_0 = 1/\tau_0 = 2\pi f_p$ . The velocity  $c$  in these equations corresponds to the unrelaxed or high-frequency limit velocity.

The complex velocity associated with eq. (B1) is

$$\bar{c}(f) = c \sqrt{\frac{if/f_0 + 1/\phi}{if/f_0 + \phi}}, \quad \phi = Q^{-1} + \sqrt{1 + Q^{-2}} \quad (\text{B3})$$

The phase velocity is  $c_p = 1/\text{Re}(1/\bar{c})$ , and the relaxed (low-frequency) velocity is  $c/a$ . This model describes attenuation of the wavefield and velocity dispersion.

The numerical algorithm to solve eq. (B1) is based on the Fourier pseudo-spectral method for computing the spatial derivatives and a fourth-order Runge–Kutta technique for calculating the wavefield recursively in time (e.g. Carcione 2014).